

## Resonant behavior in heat transfer across weak molecular interfaces

Sophia R. Sklan, P. Alex Greaney, and Jeffrey C. Grossman

Citation: *Journal of Applied Physics* **114**, 234308 (2013); doi: 10.1063/1.4851035

View online: <http://dx.doi.org/10.1063/1.4851035>

View Table of Contents: <http://scitation.aip.org/content/aip/journal/jap/114/23?ver=pdfcov>

Published by the [AIP Publishing](#)

### Articles you may be interested in

[Role of direct electron-phonon coupling across metal-semiconductor interfaces in thermal transport via molecular dynamics](#)

*J. Chem. Phys.* **143**, 034703 (2015); 10.1063/1.4922893

[A detailed microscopic study of the heat transfer at a water gold interface coated with a polymer](#)

*Appl. Phys. Lett.* **106**, 093113 (2015); 10.1063/1.4913905

[Enhanced heat transfer through filler-polymer interface by surface-coupling agent in heat-dissipation material: A non-equilibrium molecular dynamics study](#)

*J. Appl. Phys.* **114**, 193512 (2013); 10.1063/1.4831946

[Influence of surface characteristics on scattering behavior in Couette flow with heat transfer](#)


*AIP Conf. Proc.* **1501**, 1152 (2012); 10.1063/1.4769671

[A molecular dynamics study on heat transfer characteristics at the interfaces of alkanethiolate self-assembled monolayer and organic solvent](#)

*J. Chem. Phys.* **130**, 074706 (2009); 10.1063/1.3077315



# Instruments for Advanced Science

<p>Contact Hiden Analytical for further details:  <a href="http://www.HidenAnalytical.com">www.HidenAnalytical.com</a>  <a href="mailto:info@hiden.co.uk">info@hiden.co.uk</a></p> <p><b>CLICK TO VIEW</b> our product catalogue</p>	 <p><b>Gas Analysis</b></p> <ul style="list-style-type: none"> <li>› dynamic measurement of reaction gas streams</li> <li>› catalysis and thermal analysis</li> <li>› molecular beam studies</li> <li>› dissolved species probes</li> <li>› fermentation, environmental and ecological studies</li> </ul>	 <p><b>Surface Science</b></p> <ul style="list-style-type: none"> <li>› UHV TPD</li> <li>› SIMS</li> <li>› end point detection in ion beam etch</li> <li>› elemental imaging - surface mapping</li> </ul>	 <p><b>Plasma Diagnostics</b></p> <ul style="list-style-type: none"> <li>› plasma source characterization</li> <li>› etch and deposition process reaction</li> <li>› kinetic studies</li> <li>› analysis of neutral and radical species</li> </ul>	 <p><b>Vacuum Analysis</b></p> <ul style="list-style-type: none"> <li>› partial pressure measurement and control of process gases</li> <li>› reactive sputter process control</li> <li>› vacuum diagnostics</li> <li>› vacuum coating process monitoring</li> </ul>
--	--	--	--	--

# Resonant behavior in heat transfer across weak molecular interfaces

Sophia R. Sklan,<sup>1,a)</sup> P. Alex Greaney,<sup>2,3,a)</sup> and Jeffrey C. Grossman<sup>2,b)</sup>

<sup>1</sup>*Department of Physics, Massachusetts Institute of Technology, Cambridge, Massachusetts 02139, USA*

<sup>2</sup>*Department of Materials Science and Engineering, Massachusetts Institute of Technology, Cambridge, Massachusetts 02139, USA*

<sup>3</sup>*School of Mechanical, Industrial, and Manufacturing Engineering, Oregon State University, Corvallis, Oregon 97331, USA*

(Received 20 September 2013; accepted 4 December 2013; published online 19 December 2013)

Molecular dynamics (MD) simulations are used to study, in detail, the transfer of thermal (vibrational) energy between objects with discrete vibrational spectra to those with a semi-continuum of spectra. The transfer of energy is stochastic and strongly dependent on the instantaneous separation between the bodies. The insight from the MD simulations can be captured with a simple classical model that agrees well with quantum models. This model can be used to optimize systems for efficient frequency selective energy transfer, which can be used in designing a chemical sensor through nanomechanical resonance spectroscopy. © 2013 AIP Publishing LLC. [<http://dx.doi.org/10.1063/1.4851035>]

## I. INTRODUCTION

Heat transport at the molecular scale often involves exchange of energy between molecules with only slightly overlapping vibrational spectra. The frequencies at which overlap is strongest act as efficient channels for energy exchange. That this transfer is not uniform at all frequencies results in an athermal phonon population (APP) in the participating objects. Usually these are rapidly dissipated internally, however in nanoscale systems far-from-equilibrium there are a large number of cases where this phonon inversion can persist and in doing so greatly alter the system's electro-mechanical properties in ways that can be both detrimental or desirable in NEMS devices.

An APP can arise in suspended carbon nanotube (CNT) resonators through either frequency specific Joule heating of optical phonons (at K and  $\Gamma$ )<sup>1–4</sup> or direct driving<sup>5,6</sup> (or cooling<sup>7</sup>) of low frequency flexural modes. In the former case this causes the electrical conduction to saturate at high voltage, and in the latter the resulting APP can dramatically reduce the resonator's quality factor.<sup>8,9</sup> APPs can also arise when heat is conducted across CNT interfaces.<sup>10,11</sup> Taking advantage of the APP leads to strategies for engineering interfacial thermal conductivity,<sup>12,13</sup> and may be important in the recently discovered thermal power waves in CNTs.<sup>14</sup> Biological systems can also display non-equilibrium thermal energy distributions. Enzymatic reactions can result in a large heating of localized modes in the protein. This heat must be dissipated efficiently without denaturing the enzyme, and is transferred through a restricted set of localized vibrational modes without heating the enzyme as a whole.<sup>15,16</sup> (A similar concept is important for barrierless thermomolecular reactions.) A similar “energy funneling” phenomenon is observed in virus capsids<sup>17</sup> in which laser heating of high frequency modes is funneled into a handful of

low frequency mechanical modes—an effect that may be exploited for selectively destroying harmful viruses.<sup>18</sup>

A further and beneficial application of thermal transport induced APP that motivates the present work is the possibility of taking advantage of it to develop new label-free and ultra sensitive chemical sensor. We previously reported this concept, referred to as nanomechanical resonance spectroscopy (NRS),<sup>19</sup> in which an array of tuned nanomechanical resonators could become excited in the presence of a hot analyte with a particular vibrational frequency. (Figs. 1(a) and 1(b) illustrate the NRS concept and its comparison to optical spectroscopy.) Taken together, the array of resonators can be likened to a stringed musical instrument; the vibrational spectrum of each analyte strikes a unique chord that can be used to identify it. Sensing the analyte is then reduced to resolving the relative excitations of the nano-resonator array. This task of “listening” to the strings is itself nontrivial; it requires being able to measure an excitation in a single vibrational mode of an ultra-high frequency resonator, with nanosecond resolution.

In this work, we build upon the initial NRS concept by considering multiple analytes (as opposed to a single analyte) and determining the limiting resolution of the NRS method. To this end, classical molecular dynamics (MD) simulations were performed on an idealized test system representing the analytes interacting with a NRS resonance probe. These simulations were analyzed in detail using a mode projection scheme.<sup>20</sup> The insight gained from these simulations was used to develop a simple model of resonant energy transfer, from which we identified a set of parameters that determined the fundamental limits of sensitivity and selectivity of the NRS approach.

## II. CALCULATIONS

### A. Molecular dynamics simulation

The thermal transfer in the coupled analyte-resonance probe system was represented by a collection of hot, hydrogen-like diatomic molecules (whose vibrational

<sup>a)</sup>S. R. Sklan and P. A. Greaney contributed equally to this work.

<sup>b)</sup>Author to whom correspondence should be addressed. Electronic mail: [jcg@mit.edu](mailto:jcg@mit.edu)

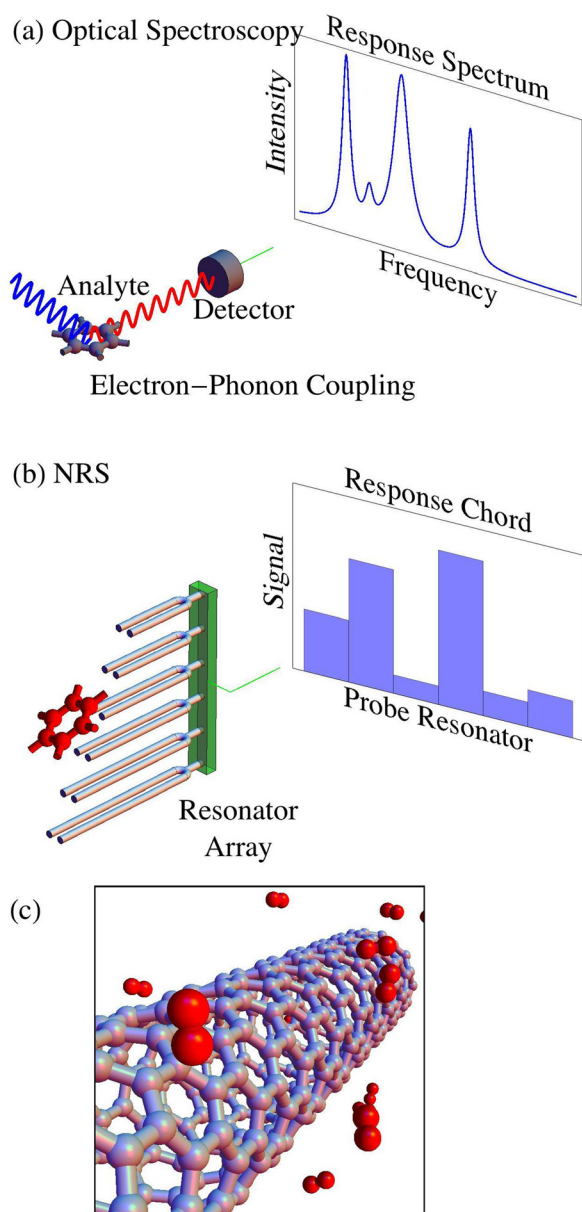


FIG. 1. A schematic comparison of NRS with traditional optical spectroscopy. Panel (a) depicts in very general terms an optical spectroscopy method, in which the vibrational modes of an analyte are interrogated with a laser. Electron-phonon coupling transduces the illuminating radiation and the measured spectrum that results is used to identify the analyte. Panel (b) depicts the proposed NRS method in which a heated analyte interacts directly with a series of nanomechanical probe resonators. If a probe is in resonance with a vibrational mode in the analyte, then vibrational energy is exchanged; thus, the analyte excites a unique chord in the array of probes which can be used to identify it. (c) Image depicting the initial configuration for one particular simulation with fifteen dimers. Panels (a) and (b) reprinted with permission from P. A. Greaney and J. C. Grossman, *Nano Lett.* **8**, 2648 (2008). Copyright 2008 American Chemical Society.<sup>19</sup>

frequency was tuned to the desired resonance by varying their atomic mass) interacting with a cold single-walled (10,0) zig-zag CNT with a 4.1 nm periodic repeat distance (10 repeated units, total length 41 nm). A typical simulation proceeded as follows: (1) After optimizing the CNT (both respect to the atomic positions and the periodic repeat distance), the CNT was heated (and equilibrated) to an initial temperature  $T_{bg}$ . (2) A random combination of dimers configurations were selected from a set of pre-computed trajectories of a single dimer

interacting with a CNT. These were distributed randomly around the CNT but placed such that the distance between the closest atom and the surface of the tube is  $d_o$ , as shown in Figure 1. Dimers were treated as hydrogen-like for modeling the interactions but with mass increased to achieve the desired resonance. (3) By a random combination of potential energy (inter-atomic displacement) and kinetic energy (instantaneous relative velocity) the dimers were initially excited to 0.32 eV of total energy in the bond-stretching mode (and no energy in the others<sup>21</sup>). (4) The system was then simulated in the micro-canonical ensemble using the velocity Verlet algorithm with a time step of 0.2 fs, limiting fluctuations in the total energy to less than  $10^{-5}$  of the mean thermal energy. The interactions between atoms were modelled using the adaptive intermolecular reactive empirical bond order (AIREBO) potential<sup>22</sup> implemented in the Large-scale Atomic/Molecular Massively Parallel Simulator (LAMMPS) molecular dynamics code.<sup>23</sup> AIREBO potential treats the (anharmonic) covalently bonded interactions internal to both the CNT (carbon-carbon bonds) and the dimers (hydrogen-hydrogen bonds), as well as the non-bonded van der Waal's interactions between the CNT and dimers. The latter interactions are treated within the AIREBO scheme as a (highly anharmonic) 12-6 Lennard-Jones potential, and it is through this interaction that the analyte molecules transfer their vibrational energy to the CNT (as well as to other dimers). A projection scheme (described in Ref. 10, integrated into the MD simulation in Ref. 20, and used previously by Kidera *et al.*<sup>15</sup>) was used to track how this transferred heat was distributed across the full vibrational spectrum of the CNT at every instant during the course of each simulation.

The excitation of the CNT resonance probe due to the interaction with just a single analyte dimer is shown in Figure 2(a). This plot shows the dissipation of thermal energy into all the vibrational modes in the CNT over the simulation duration. The plotted data are the average from 29 separate simulations in which the bond stretching mode of the dimer is tuned to have a frequency of 10.0 THz.<sup>24</sup> It can clearly be seen that energy is transmitted most favorably to modes in the CNT in resonance with the dimer, that is, modes with frequencies close to 10.0 THz, in agreement with our initial proof of concept results for NRS.<sup>19</sup> These resonant modes in the CNT are the first and most strongly excited modes, reaching a peak intensity at between 3 and 4 ns, after which the intensity diminishes slowly. In addition to the resonant excitation at 10.0 THz, there are two other sets of minor excitations that also begin from the outset of the simulation: excitation of modes at 20.0 THz and low frequency excitations below 2.0 THz. The first of these arises from the overtone of the dimer oscillation and due to frequency doubling of the dimer oscillation through the anharmonicity of the van der Waal's interaction. With its initial excitation energy (0.32 eV) the dimers overtone is approximately 7% of its oscillation. The second minor excitation is caused by low frequency oscillation of the dimer within the attractive van der Waal's potential well at the CNT surface—we refer to this motion as the analyte bouncing on the tube. The other modes in the CNT accumulate energy more gradually as the simulation progresses as can be seen in the higher frequency modes.



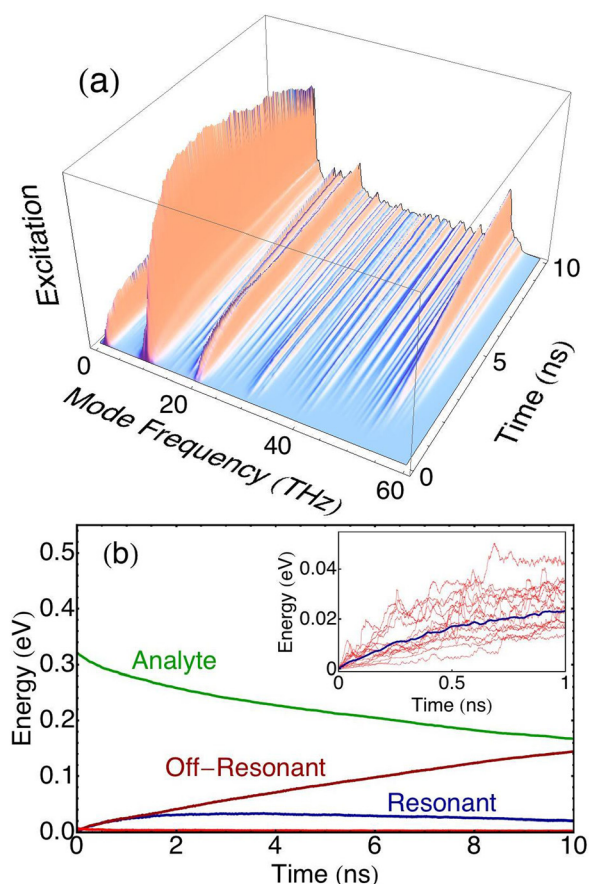


FIG. 2. Mean excitation of CNT due to interaction with a single dimer vibrating at 10 THz. The plots are the average of 29 simulations. Plot (a) shows the full excitation spectrum in the CNT. A clear resonant peak is visible at 10 THz. Plot (b) shows the partitioning of the thermal energy between the internal mode (green) and rotational and translational modes (red) of the analyte, and the resonant modes (blue) and background modes (dark red) in the CNT. The inset plot shows the first nanosecond of resonant signal for the first 15 individual simulations. It can be seen that the trajectories are stochastic, with energy repeatedly exchanging back and forth between the dimer and CNT.

It is instructive to consider the vibrational energy in the CNT to be comprised two parts, a thermal background (with an equilibrium filling of the vibrational spectrum—which for these simulations is classical) and an athermal phonon population which is localized in frequency space. For the application of NRS, the height and width of the athermal population determine the sensitivity and selectivity that can ultimately be attained with this method. The narrowness of the resonant peak determines how accurately we can resolve the frequency of the analyte's mode that is causing it. The height of the distribution—how much hotter the resonantly excited modes are than the thermal background—determines the minimum sensitivity that is required of a measurement in order to detect the APP. The shape and size of the athermal distribution in the CNT are determined by the competition of efficient energy transfer to the CNT at specific resonant frequencies and the internal relaxation of this energy into other modes in the tube.

As a simple metric of the resonant APP and thermal background we select the set of modes that participate in the resonant peak in Fig. 2(a), summing the total energy in this set approximates the energy of the APP. We refer to this as

the “resonant signal” in the CNT. The set of “resonant” modes in the CNT was chosen to be those within 0.4 THz of dimer frequency—just wide enough to enclose the full resonant APP peak, and the summing procedure amounts to a narrow bandpass filtering of the full vibrational spectrum. The equilibrium background energy is approximated by summing the energy of all the modes not in the resonant set. It should be noted that these quantities only approximately represent the height of a nonequilibrium phonon population; however, they permit one to compare rates on energy transfer from the analyte to resonance and background modes. Fig. 2(b) shows the partitioning of the total vibrational energy in the system between the resonant and background modes of the CNT, and the internal and block modes of the dimer. It can be seen that in the 10 ns simulated, less than half of the energy in the dimer's stretch (green line) has transferred to the CNT, and very little energy is transmitted into the dimer's rotational and translational modes (due to the atomic mass of the dimer being relatively large). The energy lost from the dimer is transmitted to the CNT, with the background modes showing a continuous heating, while the energy in the resonant signal shows an initial rise that saturates after about 2 ns.

The inset plot in Fig. 2(b) shows the first nanosecond of the resonant signal in the CNT for 15 individual simulations (red) with the mean signal (blue). It can be seen that the excitation of the resonant modes in each simulation follows markedly varied trajectories, but all of the trajectories show rapid fluctuations, not dissimilar from a random walk. This noisy heating indicates that energy is randomly exchanged between the analyte and CNT, with only a gradual net accumulation of energy in the CNT. The fluctuations in the transfer of energy can reveal the pathway for energy transfer. Figure 3 shows the cross-correlation (a) and power spectrum (b) of the energy fluctuations during a single simulation. The fluctuations are computed as the deviation from a running average and the correlation plot shows the Pearson correlation computed as a function of the windowing duration for the running average.

The energy fluctuations in the dimer's stretch mode are strongly anti-correlated with the fluctuations in the energy of the CNT-resonant modes. This indicates that energy leaving the dimer stretch mode often shows up in the CNT stretch. There is a similarly strong anti-correlation between the resonant and background modes of the CNT while crucially there is no significant correlation between the dimer stretch and the CNT-background modes. This indicates that while the majority of the transferred energy ends up in the CNT-background it is first transferred into the resonant modes of the CNT before dissipating into the background. This is an important result for a NRS chemical sensing device: It indicates that the system retains a high efficiency in the transfer of information about the vibrational spectrum of the analyte. Information is lost by intra-tube dissipation within the CNT rather than in the exchange process.

## B. Classical analytic model

The insight gained from the MD simulations can be captured by a highly simplified model in which one considers

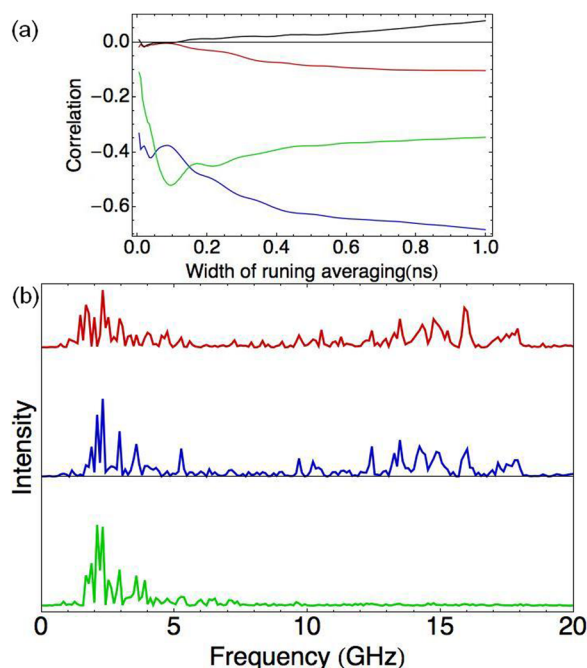


FIG. 3. Plot (a) shows the Pearson cross correlation (with blue, red, green, and black lines correspond to dimer–CNT–resonant correlation, dimer–CNT–background correlation, CNT–resonant–CNT–background correlation, and CNT–resonant–dimer rotational and translational mode correlation, respectively), plotted as a function of the windowing size of the moving average to show that the analysis is robust. Plot (b) shows the power spectrum of the energy transfer fluctuations with the energy in the dimer stretch, CNT–resonant modes, and CNT–background modes plotted in green, blue, and red, respectively. It can be seen that the transfer fluctuations in the dimer and CNT–background modes occur in different frequency bands.

the transfer of energy between a pair of weakly coupled harmonic oscillators, as shown in Fig. 4, and parametrized by three dimensionless quantities,  $\alpha$ ,  $\beta$ , and  $\gamma$  that describe, respectively, the masses, frequencies and coupling stiffness of the system (also defined in Fig. 4).

### Dimensionless parameters

$$\alpha = \frac{m_p}{m_a}$$

$$\beta = \frac{\omega_p}{\omega_a}$$

$$\gamma = \frac{\kappa_c}{m_a \omega_a^2}$$

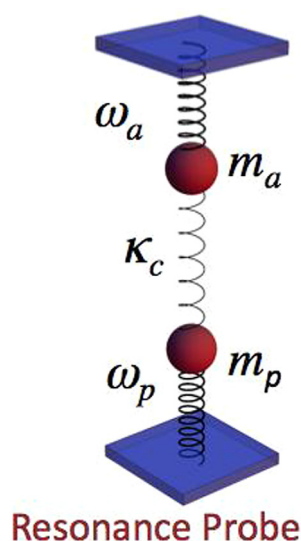


FIG. 4. Model of the transfer of energy between two coupled harmonic oscillators parametrized by the dimensionless parameters  $\alpha$ ,  $\beta$ , and  $\gamma$  which give, respectively, the ratio of the oscillators masses, the ratio of the natural frequencies, and the ratio of the coupling stiffness to the analyte's stiffness. This model is a generalization of a similar model that we have developed previously.<sup>10</sup>

The key feature of this model is that kinetic energy is transferred *without* any vibrational scattering but as a consequence of the beating of the two eigenmodes of the *coupled* system. It is assumed that scattering of the system does occur—with an average interval  $\tau$ , analogous to a phonon life-time—and acts to hinder the transfer of heat. We assume that the oscillators are decoupled during scattering events, so that the scattering in the oscillators is uncorrelated and no kinetic energy is exchanged. This model of molecular level energy transfer stands in contrast to models of heat transfer across interfaces in bulk materials in which heat is conducted by propagating vibrations that scatter as they cross the boundary.

The two harmonic oscillators are assumed to be initially uncoupled with energies  $E_a, E_p$ , and random phase  $\phi_a, \phi_p$ . Coupling the system (and neglecting the small amount of energy in the interaction potential)  $E$  and  $\phi$  are used to define the initial amplitude and phase of the eigenmodes of the *coupled* system. Propagating these eigenmodes in time one can compute  $E_a(\tau), E_p(\tau)$ , the energy in each oscillator when the system is decoupled after time  $\tau$  and before the phase of each oscillator is randomly scattered, then recoupled to transfer energy once more. During each interval that the oscillators are coherently coupled energy can be transferred either forwards or backwards depending on the initial random phases,  $\phi_a$ , and  $\phi_p$ . This matches the random trading of energy observed in our MD simulations as seen in the individual heating trajectories in the inset plot of Fig. 2(b). The average rate of energy transfer,  $\langle \dot{Q}_{ap} \rangle$ , from all possible starting configurations is obtained by integrating  $\phi_a$ , and  $\phi_p$  over the interval 0 to  $2\pi$ . Strictly one should also average over a distribution of scattering intervals  $\tau$ . Here, we chose to ignore this—proceeding assuming  $\tau$  to be single valued—and rationalize this decision later in the paper. The expression obtained for the rate of energy transfer permits the definition of a “mean dimensionless energy transfer efficiency” given by the approximation

$$R_{ap} = \frac{\langle \dot{Q}_{ap} \rangle}{\omega_a(E_a - E_p)} \approx \frac{L}{2\pi\eta} \left( 1 - \cos\left(\frac{\omega_b}{\omega_a} 2\pi\eta\right) \right). \quad (2.1)$$

Here,  $R_{ap}$  is the fraction of the energy difference that is transferred per analyte oscillation divided by  $2\pi$  and can be considered analogous to the quality factor of a resonator ( $\langle \dot{Q}_{ap} \rangle$  is the averaged rate of heat transfer). The dimensionless term  $\eta = \tau\omega_a/2\pi$  expresses the coupling coherence time as the number of analyte oscillations, and  $\omega_b$  is the beat frequency (i.e., the difference in frequency) of the two eigenmodes of the coupled system

$$\omega_b = \frac{\omega_a}{\sqrt{2\alpha}} \left( \sqrt{Y - \sqrt{X}} - \sqrt{Y + \sqrt{X}} \right), \quad (2.2)$$

with terms

$$X = \gamma^2 + \alpha^2(\gamma + 1 - \beta)^2 + 2\alpha\gamma(\gamma - 1 + \beta^2), \quad (2.3)$$

$$Y = \gamma + \alpha(1 + \beta^2 + \gamma).$$

The leading term,  $L$ , in Eq. (2.1) is a Lorentzian function

$$L = \frac{1}{\pi} \frac{\Delta\beta}{(\beta - \beta^*)^2 + \Delta\beta^2}, \quad (2.4)$$

centered at  $\beta^* = \sqrt{1 + \gamma - \gamma/\alpha}$ , and with width at half maximum  $\Delta\beta = -2\gamma/\sqrt{\alpha}$ .

Before interpreting the implications of the derived expression (2.1), it is worthwhile taking a short detour to justify the use of this highly simplified two-oscillator system to model the analyte-probe energy transfer process—and to underscore the merits of doing so. A real coupled analyte and probe system involves a hybrid set of eigenmodes found by diagonalizing a matrix of the form

$$\mathbf{H} = \begin{vmatrix} \lambda_a & 0 \\ 0 & \lambda_p \end{vmatrix} + \begin{vmatrix} \mathbf{K}_a & \mathbf{\kappa}_{ap} \\ \mathbf{\kappa}_{pa} & \mathbf{K}_p \end{vmatrix}, \quad (2.5)$$

where  $\lambda_a$  and  $\lambda_p$  are the diagonal matrices of eigenmode stiffnesses for the decoupled system, and  $\mathbf{\kappa}_{ap}$  is the matrix of coupling stiffnesses of modes in the analyte to modes in the probe.  $\mathbf{K}_a$  and  $\mathbf{K}_p$  are diagonal matrices of mode stiffening due to the probe-analyte interaction and are the column or row sum of  $\mathbf{\kappa}_{ap}$ . Only hybrid modes that contain large contributions from both the probe and analyte will participate in the transfer of energy. In practice, if the coupling matrix,  $\mathbf{\kappa}_{ap}$ , is weak most modes will be relatively unchanged with only collections of modes close by in frequency hybridizing, as evidenced by the cross-correlation analysis in Fig. 3 (conversely, when  $\mathbf{\kappa}_{ap}$  is large, mode mixing and stiffening can result in many modes becoming resonant). Thus, the presence of  $\mathbf{\kappa}_{ap}$  justifies ignoring most of the modes in the system and only considering modes that are shared between the analyte and probe. There are considerably more than two shared modes—22 modes contribute to the what we call the “resonant signal” in Fig. 2 (Ref. 25)—however, considering only two modes considerably simplifies the mathematical treatment of the problem while still capturing the essential physics, and can lend insight to more realistic energy transfer processes (we gain the most insight for the least amount of mathematical effort). Armed with understanding of the two-oscillator model one can predict trends in the behavior of the model as more participating modes are considered without finding the full-blown analytic solutions for these more intricate systems. There are two main limitations to the overly simplified model: First that caution must be used when making direct comparisons with the MD simulation results, and second that one cannot easily include quantum mechanical effects.

### C. Quantum analytic model

The second limitation can be mitigated by comparing the results of the classical model with those of a simple quantum model. The classical harmonic oscillators considered previously now become quantum harmonic oscillators. To include the effects of scattering, these harmonic oscillators are coupled by a time-dependent potential. The time dependence is idealized as a square pulse of width  $\tau$

beginning at  $t=0$ . Thus, the perturbation can be written as  $\frac{\Theta(t)\Theta(\tau-t)}{2}\kappa_i(x_i - x_0)^2$ , where  $x_i$  is the amplitude of the nanotube mode and  $x_0$  is the amplitude of the analyte mode (this notation is adopted to ease the extension to multiple nanotube modes). This problem can now be reduced to a time-dependent perturbation theory problem, where we will retain terms to  $O(\tau)$ . The coupling includes both diagonal and off-diagonal elements. The former terms shift the frequencies of the phonon modes to  $\omega_i + \kappa_i/2m_i\omega_i$  (we call these “shifted modes”). The latter terms can create or destroy pairs of phonons in any individual mode, create or destroy a single phonon in each of a pair of modes, or swap a phonon between a pair of modes. When the two shifted modes are nearly degenerate, the hopping terms dominate. Taking the norm of the forward and backward hopping amplitudes gives the probabilities of the two events, which we can use to generate the expectation value of the energy shift. Differentiating with respect to  $\tau$  gives

$$\begin{aligned} \langle \dot{Q} \rangle &= \frac{1}{2} \frac{\kappa_i}{m_i\omega_i} \frac{\kappa_i}{m_0\omega_0} (n_0 - n_i) \frac{\sin\omega_b\tau}{\omega_b} \hbar(\omega_i - \omega_0) \\ &= \frac{1}{2} \frac{\kappa_c}{m_1} \gamma \sqrt{\frac{1}{\alpha\beta}} (n_0 - n_i) \frac{\sin\omega_b\tau}{\omega_b} \Delta E \\ &\approx \frac{1}{2} \frac{\kappa_c}{m_1} \gamma \sqrt{\frac{1}{\alpha\beta}} (n_0 - n_i) \tau \Delta E, \end{aligned} \quad (2.6)$$

where  $\omega_b = (\omega_0 + \frac{\kappa}{2m_0\omega_0}) - (\omega_i + \frac{\kappa_i}{2m_i\omega_i})$ . The second equality follows by converting our notation to the classical models, and the last equality follows from the near resonance condition. This final expression is in good agreement with the classical model, differing by a factor of 2 (due to differentiating by  $\tau$  rather than dividing by  $\tau$  to convert from the total energy transfer to the  $\langle \dot{Q} \rangle$ ).

One convenience of the quantum model is the ease of including multiple modes. When more nanotube modes are added, the rate of energy transfer is unmodified except in the case that multiple shifted modes are nearly resonant with the analyte mode (this is possible even for non-degenerate modes because of the effects of coupling). In this case, the expectation value of the energy change has to run over all near-resonant modes. Other than this effect, the presence of other modes only becomes non-trivial for second order perturbations, which are negligible in the case of near-resonance. This strengthens our claim that the essential features of the CNT-dimer dynamics can be captured with a pair of coupled modes.

The derivation of the result in Eq. (2.1) is classical, as are the MD simulations that inspired it, but the premise of the model does not require a classical interpretation. Vibrational energy is transferred between the analyte and probe continuously rather than discretely but without energy transitions between eigenmodes. The skulduggery occurs in how the modes are decoupled. In the classical derivation of Eq. (2.1) it is assumed that decoupling does not change the energy of each individual oscillator, and then when they are recoupled all phases are equally likely. In a quantum mechanical system, after the analyte and probe have been



decoupled the isolated modes must be discretely populated, and the scattering must obey energy conserving phonon selection rules. The same applies when the system is subsequently recoupled. The two-oscillator model is overly restrictive and has no other degrees of freedom (such as translation, or additional vibrations) that can participate in the required energy redistribution when coupling/decoupling the quantum oscillators. In a model in which more participating modes are considered, this restriction is relaxed.

### III. DISCUSSION

With the goals and limitations of the oscillator model of energy transfer in mind we return to discussing the implications of Eq. (2.1), for understanding both the simulation results and NRS approach to chemical sensing. The surface plot in Fig. 5 shows the energy transfer efficiency  $R_{ap}$  plotted as a function of dimensionless probe frequency,  $\beta$ , and the dimensionless coherence duration,  $\eta$ . Although, this plot relates the efficiency of energy transmission between two coupled oscillators as a function of their mismatch in frequency, it may be interpreted as the heating spectrum across all the modes of a large resonance probe in a NRS device, such as the CNT in the MD simulations. The surface may also be interpreted as the sensitivity of a selected mode in the probe to analytes of different frequency. A striking feature in Fig. 5 is that modes in the probe that are heated most strongly are not those that are exactly in resonance with the analyte, but those at the slightly higher frequency  $\beta^* = \sqrt{1 + \gamma - \frac{\gamma}{\alpha}}$ . This seemingly off-resonant interaction is due to the differences in masses of the probe and analyte: As the analyte is lighter than the probe, its frequency is more sensitive to the stiffening effect of the coupling. The analyte frequency is raised into resonance with higher frequency modes in the probe, and thus we still refer to this as *resonant* energy transfer. Importantly for NRS sensing, it means that resonance probes must be tuned slightly above the pitch of the analyte modes for light target species.

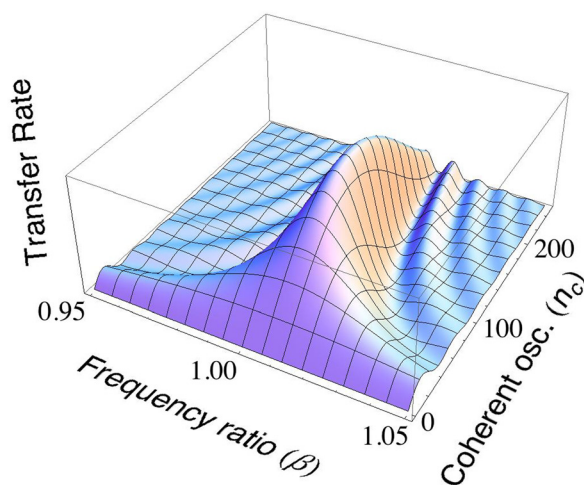


FIG. 5. Surface plot of the dimensionless energy transfer rate,  $R_{ap}$ , from the model (Eq. (2.1)) plotted as a function of dimensionless probe frequency,  $\beta$ , and number of oscillation for which the coupled system remain coherently coupled and unperturbed,  $\eta$ , computed for mass ratio  $\alpha = 14$ , and dimensionless coupling  $\gamma = 0.01$ .

In the NRS chemical recognition devices outlined at the beginning of this paper, one envisions monitoring for excitations in modes at one frequency in a large (relative to the analyte) nanoscale resonator, such as a CNT, or graphene membrane. The measurable excitation in the probe (the APP) results from the balance of energy transfer and internal dissipation. To maximize the sensitivity of the device, one must maximize the rate of energy transfer into these monitored modes. The selectivity of the NRS device is limited by how finely it can resolve analyte frequency, and thus to optimize selectivity one must minimize the energy transfer from modes just off-resonance. In Fig. 5,  $R_{ap}$  is plotted against the interaction time  $\eta$  (for a given value of  $\alpha$  and  $\gamma$ ). It can clearly be seen that there are optimal values of  $\eta$  that maximize the rate of energy transfer, thereby focusing the transfer spectrum<sup>26</sup> (for a given value of  $\alpha$  and  $\gamma$ ). While not coincident, these optimal  $\eta$  are close together, and the peak rate of energy transfer is only slightly diminished where frequency resolution is maximal. If we assume that there are things that we can do to a NRS system to engineer  $\eta$ , then this is an encouraging result. It means that when the device design is optimized, there need be little trade-off between selectivity and sensitivity.

In order to make use of these ideas for optimizing a realistic NRS system, we make the following mapping ansatz: While the two-oscillator model does not describe a realistic system there are a set of values of  $\{\alpha, \beta, \gamma, \eta\}$  that make the oscillator model best represent the real system. If we can find these effective parameters, then we can use optimization of our model to direct optimization of the real system. In practice, this means that if we wish to alter a system (such as the test system used in the MD simulations) to improve energy transfer we must first identify which point on the plot in Fig. 5 best represents the system. The following discussion addresses this mapping for the CNT/dimer system of the MD simulations.

In bulk heat transport, scattering is a stochastic process in which the phonon life time  $\tau$  is the average time it takes phonons to collide or to encounter scattering centres. In the MD simulations of frequency dependent heat transfer, the scattering or decoupling time has an entirely different origin. As an analyte dimer interacts with the CNT it is trapped and bouncing around in the highly anharmonic van der Waals potential well at the CNT surface. The strength of coupling between the internal modes of the analyte and the probe depends on the local curvature of the van der Waals potential well, which is highly asymmetric. As the analyte bounces around on the surface of the probe, the coupling of its modes to the probe varies greatly—as we showed previously<sup>19</sup> the coupling is strongest during the nadir of the bounce when the analyte is sampling the stiff, repulsive, part of the potential well. When the coupling is strongest, the most rapid exchange of energy occurs (either forward or backward). This can be seen in Fig. 6, which shows the conditional probability distribution of the gradients in the resonant signal at different CNT-dimer separations. The inset contour plot shows the full probability density from which the slices are taken.

It can clearly be seen that the largest changes in signal (i.e., the fastest energy exchange) occur when the analytes

are closest to the probe. In this system, the analyte bounces on average once every  $\tau_{bnc} = 2.8 \pm 0.2$  ps,<sup>27</sup> or every 28 oscillations of its stretch mode. During the period of closest approach the dimer is strongly coupled, and exchanges heat with the CNT but as the dimer rebounds away from the tube the coupling is greatly diminished. When the dimer approaches the tube again it does so in a different position with different orientation, and the resulting hybrid modes of the newly recoupled system are different. This slow bouncing oscillation is doing two things: It sets the timescale for the coupling between the analyte and probe—that is, the 5–10 oscillations that they are closest—but it also introduces a waiting time between periods of strong coupling where there is little energy transfer. In effect, scattering is not instantaneous but is actually slower than the coupling duration. The energy transfer time is a fraction of the full bouncing period  $\tau = f\tau_{bnc}$ , and the expression in the rate of energy transfer in Eq. (2.1) needs to be rescaled by  $f$ . Rather than being a random process the coupling is metronomically regulated by a much slower oscillation. The distribution of  $\tau$  is closer to being single-valued, as we assumed in deriving Eq. (2.1), than an exponential Poisson distribution of waiting times.

Understanding the origin of  $\eta$  one can identify ways to change it. Increasing the mass of the analyte will increase the interaction time, as will reduce the depth of the van der Waal's potential.

To map the coupled-oscillator model onto the MD data, we need to extract effective model parameters from the simulations. The mass ratio  $\alpha$  is computed directly as the ratio of the mass of the modal inertias. To tune the frequency of the H<sub>2</sub> dimer down to 10.0 THz, the mass of the H atoms has been artificial increased resulting in  $\alpha = 14.8$ . The frequency mismatch between the resonance modes and analyte modes was determined from the position of the resonant peak in Fig. 2(a) and found to be  $\beta = 1.03$ . Using the expression for  $\beta^* = \sqrt{1 + \gamma - \gamma/\alpha}$ , these give an effective stiffness of  $\gamma = 0.065 \pm 0.005$ . Replotting  $R_{ap}$  computed with these values (shown in Fig. 7), we see that most efficient energy transfer occurs with  $\eta$  in the range of 20–25. The effective  $\eta$  in the simulation data is estimated to be between 10 and 15. The width of the peak in Fig. 7 in a slice taken at  $\eta = 15$  is

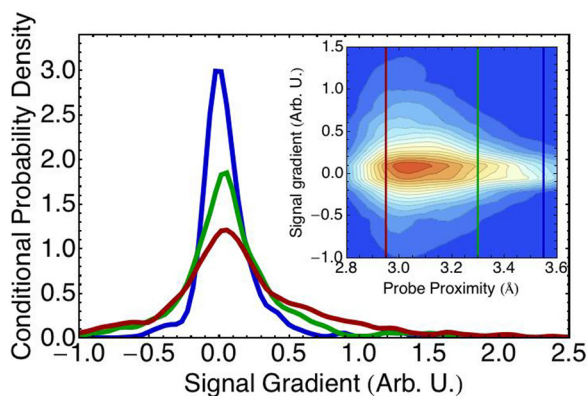


FIG. 6. Image depicting the conditional probability distribution of the given signal gradient for different values of the instantaneous probe-analyte proximity. The inset plot shows the full 2-dimensional probability of which the main plot are normalized slices.

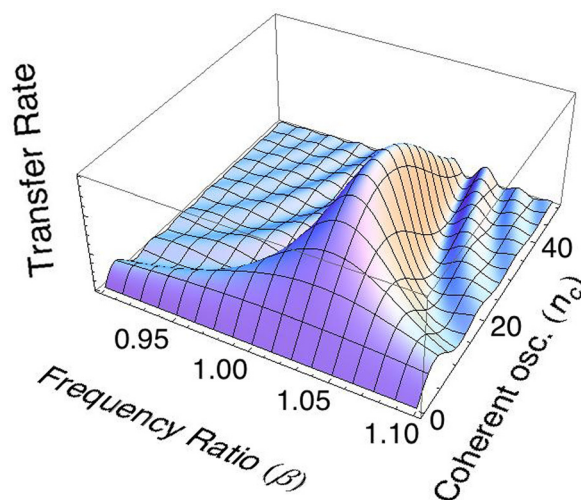


FIG. 7. Surface plot of the dimensionless energy transfer rate,  $R_{ap}$ , from the model (Eq. (2.1)) computed for mass ratio  $\alpha = 14.8$ , and dimensionless coupling  $\gamma = 0.065$ .

consistent with the width of the resonant signal in the simulations. Together these results are encouraging: They imply that there is room to optimize the system, but that the optimal conditions do not involve coherence times many times longer than the bouncing period, and that the optimal conditions should be attainable.

While the two oscillator model represents the qualitative energy transfer behavior, the computed value of  $R_{ap}$  in Fig. 7 is nearly two orders of magnitude larger than that observed in the MD simulations. The real system consists of many modes in the CNT interacting with the analyte simultaneously. Adding degenerate oscillators to the probe side of the coupled oscillator model reduces the total rate of energy transfer. Figure 8 shows the reduction in  $R_{ap}$  as a function of increased degeneracy in the probe oscillators. The reduction in  $R_{ap}$  comes from two factors: (1) the coupling between probe and analyte is now shared between all the constituent oscillators in the probe, reducing the coupling to each individual oscillator; and (2) the constituent oscillators in the probe have random phases and thus the net force felt by the analyte is reduced by phase cancellation.

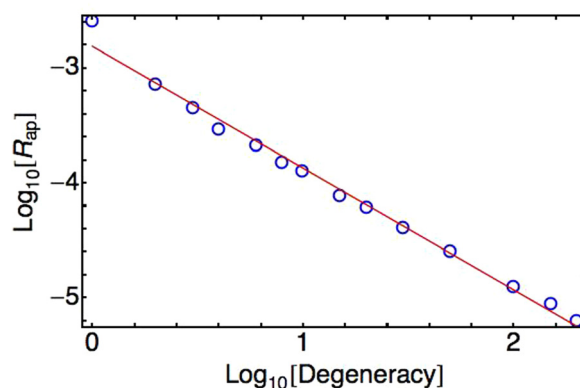


FIG. 8. Log plot showing the reduction of the energy transfer rate,  $R_{ap}$ , with increasing degeneracy of the probe resonators. The blue circles were computed numerically assuming oscillators of equal frequency and mass and using values for  $\gamma$  and  $\eta$  of 0.005 and 5, respectively. The red line shows the best fit through the computed data and has a slope of  $-1.06$ .



This observed behavior in Fig. 6 underscores the key insight from the MD simulations that energy transfer from a single dimer is stochastic: The dimer only interacts with the probe for a fraction of the time, and when it does so it is in short coherent bursts. The random phase change between periods of interaction means that the energy passed during one period of interaction can be refunded in the next, and thus the net exchange of energy follows a biased random walk.

The stochastic picture of single analyte energy exchange is the starting point for interpreting the resonance signal measured when there are multiple analyte molecules interacting with a resonance probe. The plots in Fig. 9 show the excitation of the resonance probe in the presence of multiple analyte dimers, each with a random initial position and phase. Plot (a) shows the evolution of the resonant signal. Crucially, *the signal increases with the number of dimers*, until it reaches a threshold at about 10 dimers. This result is not only an important requirement for chemical sensing but it is also contrary to what one might expect if all the dimers were interacting with the probe simultaneously. If all the analyte dimers interacted with the probe equally, phase cancellation would reduce the net force from the analyte—this is one of the effects that reduces the rate of energy transfer

when the probe contains degenerate modes as shown in Fig. 8. Instead, the combination of the block motion of the dimers in the van der Waal's potential and the potential's strong anharmonicity conspires so that only one dimer is felt by the CNT resonance probe at a time. The coupling stiffness between analyte and probe  $\kappa_c$  has a  $\sim r^{-14}$  dependence, so that the coupling of most of the dimers is negligible in comparison with the coupling to the dimer that is closest to the probe. Increasing the number of analyte molecules means that average spacing between the probe and its closest analyte will be shorter, and thus the rate of energy transfer will increase. When there is a large concentration of analytes interacting with the probes the time period for which the closest molecule remains the closest before being succeeded by another becomes short, reducing the coherence time  $\eta$ . This causes the rate of energy transfer to saturate and broadens the frequency specificity as can be seen in the time averaged spectra shown in Fig. 9(b).

#### IV. CONCLUSIONS

The results presented in this article are encouraging for the operation of a NRS device. We observe the surprising but desirable behavior that frequency dependent energy transfer increases with the concentration of analyte. A detailed study of the resonant transfer of vibrational energy between two molecular/nano-scale objects<sup>28</sup> furnished an explanation of the concentration dependence. The understanding gained from the MD simulations was used to formulate a very simple analytic model that can be used to help optimize the sensitivity and selectivity of a NRS system, and yields a second important result, that optimizing a system for sensitivity will in most cases also improve the selectivity. Finally, while this work focused on exploiting frequency dependent heat transfer for chemical sensing, the findings presented can have impact for other applications beyond NRS. These insights might be useful in the development of thermally responsive functional materials and also in the development of phononic devices such as thermal switches and thermal rectifiers.

#### ACKNOWLEDGMENTS

This project received funding from the Defense Threat Reduction Agency-Joint Science and Technology Office for Chemical and Biological Defense (Grant No. HDTRA1-09-1-0006), and National Science Foundation Graduate Research Fellowship under Grant No. 1122374. This research used resources of the National Energy Research Scientific Computing Center (NERSC), which is supported by the Office of Science of the U.S. Department of Energy under Contract No. DE-AC02-05CH11231.

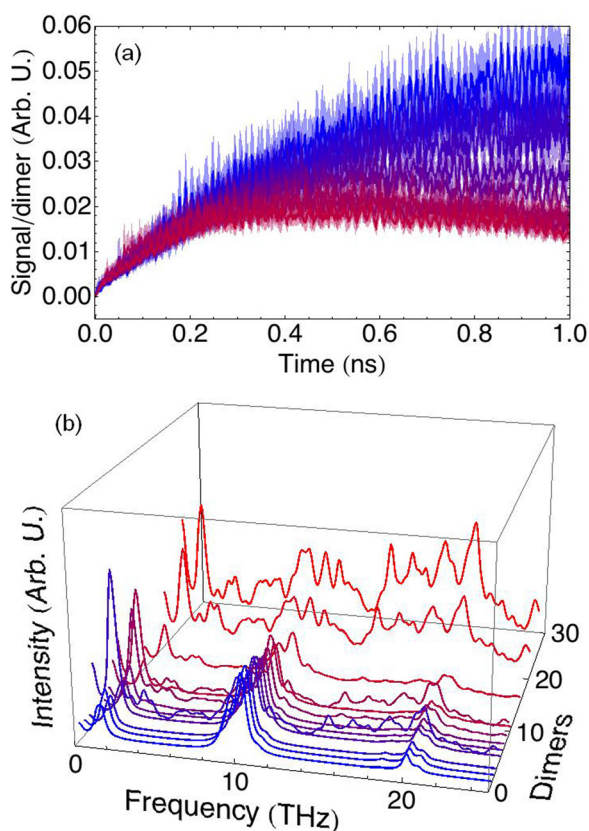


FIG. 9. Excitation of CNT resonance probe in the presence of multiple analyte dimers. (a) shows the evolution of the filtered resonant signal, normalized by the number of analytes. Coloration denotes number of analytes, from 1 (blue) to 10, plus 15, 20, and 25 (red) dimers. (b) shows the full time averaged spectra normalized by number of analytes for increasing analyte densities (averaged over first 1 ns), using the same color scheme. With greater than 10 analytes the resonant signal saturates and the resonant peak broadens, losing frequency resolution of the NRS.

<sup>1</sup>Z. Yao, C. L. Kane, and C. Dekker, *Phys. Rev. Lett.* **84**, 2941 (2000).

<sup>2</sup>M. Steiner, M. Freitag, V. Perebeinos, J. C. Tsang, J. P. Small, M. Kinoshita, M. Yuan, J. Liu, and P. Avouris, *Nat. Nanotechnol.* **4**, 320 (2009).

<sup>3</sup>M. Lazzeri and F. Mauri, *Phys. Rev. B* **73**, 165419 (2006).

<sup>4</sup>N. Vandecasteele, M. Lazzeri, and F. Mauri, *Phys. Rev. Lett.* **102**, 196801 (2009).

- <sup>5</sup>B. Lassagne, D. Garcia-Sanchez, A. Aguasca, and A. Bachtold, *Nano Lett.* **8**, 3735 (2008).
- <sup>6</sup>K. Jensen, K. Kim, and A. Zettl, *Nat. Nanotechnol.* **3**, 533 (2008).
- <sup>7</sup>A. Schliesser, P. Del'Haye, N. Hooshi, K. J. Vahala, and T. J. Kippenberg, *Phys. Rev. Lett.* **97**, 243905 (2006).
- <sup>8</sup>P. A. Greaney, G. Lani, G. Cicero, and J. C. Grossman, *Nano Lett.* **9**, 3699 (2009).
- <sup>9</sup>P. A. Greaney, G. Lani, G. Cicero, and J. C. Grossman, *Metall. Mater. Trans. A* **42**, 3907 (2011).
- <sup>10</sup>P. A. Greaney and J. C. Grossman, *Phys. Rev. Lett.* **98**, 125503 (2007).
- <sup>11</sup>S. T. Huxtable, D. G. Cahill, S. Shenogin, L. Xue, R. Ozisik, P. Barone, M. Usrey, M. S. Strano, G. Siddons, M. Shim, and P. Keblinski, *Nature Mater.* **2**, 731 (2003).
- <sup>12</sup>H. Zhong and J. R. Lukes, *Phys. Rev. B* **74**, 125403 (2006).
- <sup>13</sup>Z. Xu and M. J. Buehler, *ACS Nano* **3**, 2767 (2009).
- <sup>14</sup>W. Choi, S. Hong, J. T. Abrahamson, J.-H. Han, C. Song, N. Nair, S. Baik, and M. S. Strano, *Nature Mater.* **9**, 423 (2010).
- <sup>15</sup>K. Moritsugu, O. Miyashita, and A. Kidera, *Phys. Rev. Lett.* **85**, 3970 (2000).
- <sup>16</sup>X. Yu and D. M. Leitner, *J. Phys. Chem. B* **107**, 1698 (2003).
- <sup>17</sup>E. C. Dykeman and O. F. Sankey, *J. Phys.: Condens. Matter* **21**, 505102 (2009).
- <sup>18</sup>K.-T. Tsen, S.-W. D. Tsen, Q. Fu, T.-C. Wu, O. F. Sankey, B. Ramakrishna, J. G. Kiang, B. Karanam, S. M. Lindsay, K. Kibler, S. Jagu, R. B. S. Roden, B. Jacobs, and C.-F. Hung, *J. Biomed. Opt.* **14**, 064042 (2009).
- <sup>19</sup>P. A. Greaney and J. C. Grossman, *Nano Lett.* **8**, 2648 (2008).
- <sup>20</sup>R. Raghunathan, P. A. Greaney, and J. C. Grossman, *J. Chem. Phys.* **134**, 214117 (2011).
- <sup>21</sup>Including the center of mass translational and rotational modes. These contributions are removed to eliminate artifacts due to bringing the CNT and dimer too close together when we excite the dimer.
- <sup>22</sup>S. J. Stuart, A. B. Tutein, and J. A. Harrison, *J. Chem. Phys.* **112**, 6472 (2000).
- <sup>23</sup>S. Plimpton, *J. Comput. Phys.* **117**, 1 (1995).
- <sup>24</sup>When excited with 0.32 eV of energy, the frequency of these dimers increase approximately linearly to  $\sim 10.4$  THz as the excitation decays to zero.
- <sup>25</sup>This number is somewhat arbitrary—we could easily have included more or less. However, if we only considered interaction with just one frequency we would still have to include more than one mode as most vibrational modes in the CNT are either doubly or four-fold degenerate.
- <sup>26</sup>Maximizes the peak to width ratio of a slice along the  $\beta$  axis.
- <sup>27</sup>Computed by Fourier transforming the CNT-dimer separation.
- <sup>28</sup>Our models can also be applied to energy transfer within a molecule, provided the mode coupling is modified correctly. The MD simulations treat the coupling between resonant modes (Van der Waals) as distinct from the other couplings (covalent bonds), but this is unlikely to hold within a molecule. Both analytic models assume a finite interaction time  $\tau$  arising from the interaction being switched on and off, whereas for a single molecule there will always be interactions and  $\tau$  will instead model the life-time of the phonons. With these caveats in mind, our results should still carry over into the single molecule case, being most applicable to the examination of energy transferred between two nearly degenerate, anharmonic modes.